A novel method for skeletal age estimation based on cranial suture analysis

Documentation

Author - Andrey Gizdov*
Weizmann Artificial Intelligence Center
Weizmann Institute of Science
andrey.gizdov@weizmann.ac.il

Mentor - Stanislav Harizanov
Institute of Mathematics and Informatics
Bulgarian Academy of Science
s.harzanov@gmail.com

November 22, 2021

Abstract

The accurate age estimation is a substantial part of the integral biological profile, but quite complex in cases of unidentified decomposed and skeletonized human remains, especially in adults. Commonly, the skull is well-preserved, and due to the cranial sutures ossifying in conjunction with age, the patency of contact between adjacent calvarial bones has been used for an age-at-death prediction in the bioarchaeological and forensic expertises. Until now, the correlation between suture closure and age-at-death (AAD) has been examined by methods based on subjective assessment of the suture surface, using descriptive rank- ordered scoring scales of various grades.

This project is aimed at elaborating an algorithm for objective automatic assessment of the suture closure degree in cross-section, and assessing its relation to aging. For the purpose, volumetric images (.TIFF) of dry skulls, generated by an industrial μCT system, have been used. The obtained spatial resolution (voxel size of 97.5 μm for μCT) was high enough to allow precise detection of the suture using a VGG-16 semantic segmentation neural network with accuracy of 81%. The segmented suture area is processed using adaptive thresholding and C-Means clustering, which provides a number of important metrics used to describe the degree of suture fusion. Such metrics were recorded and analyzed for a population of 42 adult male skulls with known age-at-death. A statistically significant correlation was proven between the algorithm-measured variables and AAD, which is something that has never been done with the help of a computer algorithm so far. Furthermore, a regression equation was generated, to relate the algorithm's measurements with the age-at-death of individuals. The prediction accuracy of the regression was tested on an independent sample of skulls and showed to reduce the error of the predicted AADs over 3 times compared to the already exist methods for AAD estimation based on cranial suture analysis. The project saves human resources by completely automatizing the process of cranial suture assessment and provides a significantly more accurate age prediction than any of the existing methods in the field. Overall, this improvement is an important advancement in forensic science and archaeology, as it introduces a new objective and automatic method for age estimation in cases of unidentified skeletal remains.

1 Introduction

The human skull is made from multiple plates (bones), connected together to form a solid structure. The connections between those plates are called cranial sutures and are located at the edges of the separate bones which form the skull. Throughout physical development, they function as bone growth sites in response to the intrinsic separating forces from the growing brain requirements.

At an early stage of life, to allow for this growth, the sutures are wide and filled with a flexible soft tissue. As the individual grows up to adolescence, the plates of the skull fuse together, forming a much narrower suture path and providing the skull bones with a more solid connection over time. This change in width and shape of the sutures is

*European Union Contest for Young Scientists

directly dependent on aging, as it continues throughout the life of the developing human body. Forensic scientists and anthropologists have been using this dependency: to assess the degree of fusion along the sutures and estimate the Age-At-Death (AAD) of the skull's holder. For many years, assessing the suture has mostly been conducted on the surface level only, due to the lack of non-invasive methods for accessing the suture cross-section.

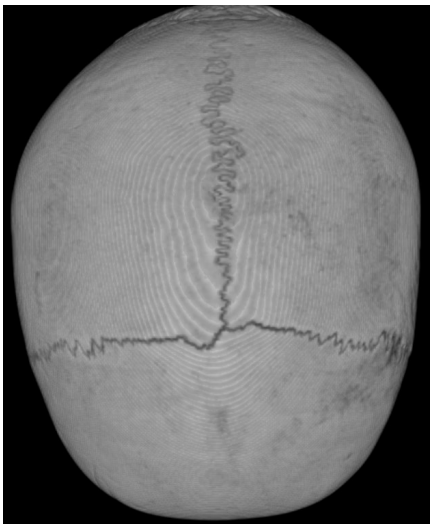

Figure 1: Suture surface view

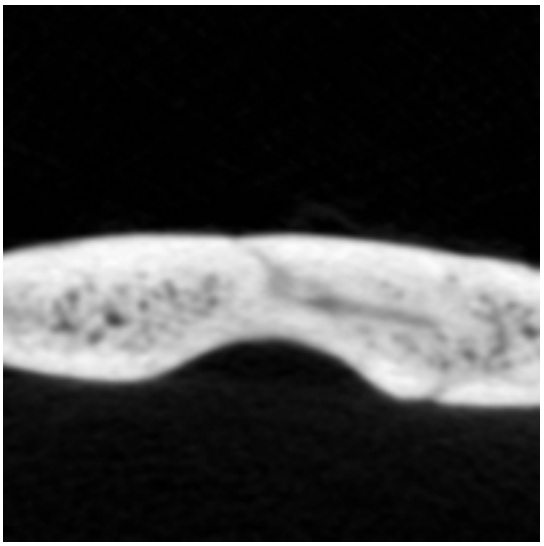

Figure 2: Suture cross-sectional view

On *Figure 1*, the surface of the suture would be given a rating of some sort, which would further be translated to an age estimate using a regression model. An example of a surface grading scale is shown on *Figure 1* in the appendix. This is type of surface assessment has a major limitation, as suture ossification often appears firstly in the core of the bone rather than the surface. Therefore, by not considering the cross-section of the suture, a lot of useful information about the degree of fusion can remain unrecorded, causing inaccuracy in the produced age estimates.
Nowadays, the increasing availability of CT scanners allows for an inside view of a skull's structure. This type of in-depth (cross-sectional) analysis of a suture is a new approach, and only three studies have been conducted on the topic. In two of the studies a human is responsible for evaluating the level of bone fusion along the suture, which is incredibly time consuming, subjective and therefore, sometimes inaccurate. There has been only one attempt to automatize this process with the use of a simple algorithm. The results were not able to prove any correlation between the degree of suture fusion and AAD, as the suture detection algorithm lacked the ability to consider many of the features which a suture can have.
In *Figure 2*, the suture can be seen as a crack passing through the bone cross-section. The algorithm's output, describing the degree of suture fusion in study [1] is only binary. On this image, the output would be '0', corresponding to a fused suture.
While the suture is very vague, it can still be seen that the bones aren't completely fused, as the suture is still distinguishable. To determine how far from complete fusion the bones are, the difference between the color intensity of the suture and the color intensity of the bone needs to be determined. A simple binary output lacks the ability to describe such information, causing the previously used algorithm to perform poorly in the task of suture assessment.
Even if a professional were to analyze the degree of suture closure on this image, while distinguishing the suture, they could never tell exactly which shade of gray along the *0 - 255* grayscale color spectrum corresponds to the mean color of the particular suture. This is important information, as a small difference in this color intensity could mean a slightly higher or lower degree of bone ossification (density). Those bits of extra information on a certain image, like the exact color intensity of the suture or the average thickness of the suture, and many others, have been neglected by all currently known techniques for age estimation. Such measurements are impossible to do by the naked human eye, but relatively easy to calculate using modern computer algorithms. Considering this extra information can be key to improving the accuracy of age estimation based on cranial sutures, with real world applications in multiple fields including archaeology, criminology and anthropology.

This project addresses the lack of accuracy and up-to-date technology in the already existing methods, by elaborating an algorithm for more accurate and objective AAD estimation, based on assessment of the suture cross-section with the help of computer science and machine learning.

2 Project process

2.1 Image generation

Typically, methods for assessment of the suture cross-section in previous studies, extract slice data by manually adjusting the intersection of planes on the 3D skull model, using an imaging software. The purpose is to correct the skull incline, so that the intersecting plane cuts exactly perpendicular to the suture surface. This results in the most accurate cross-sectional view.This is a comparison between intersecting planes producing a correct cross-sectional and a prolonged cross-sectional suture slice.

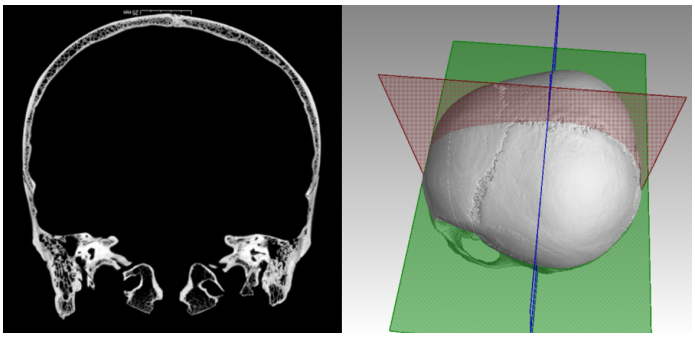

Figure 3: Perpendicular cross-sectional slice

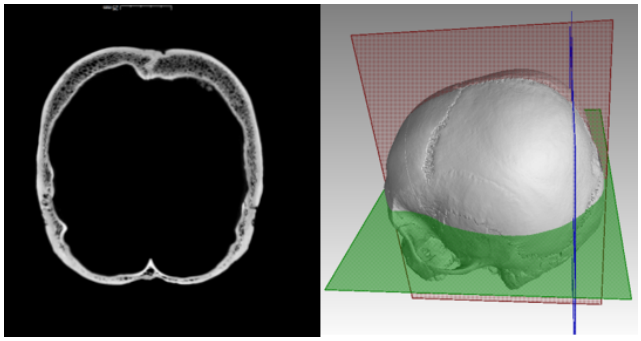

Figure 4: Prolonged cross-sectional slice

The suture cross-section on *Figure 4* appears to be very thick, when in fact it is not. This is deceiving and can not be used for reliable assessment. Furthermore, there are several issues regarding this method for data extraction:

1. It is incredibly time consuming to do on bulk quantities of skull data, since the observer has to manually adjust the skull rotation for every image along the suture length.
2. It requires very expensive hardware. To simply load an entire CT scan of a skull into a 3D imaging software like this one, approximately 64 GB of RAM memory are required. Furthermore, to run the imaging program without experiencing significant lagging, a very powerful video card is also necessary.
3. The observer is entirely responsible for ensuring that the intersecting plane is perpendicular. This is subjective and can often lead to the plane not being truly perpendicular and therefore, can cause some distortion in the produced cross-sectional slice.

The first part of the project is focused on introducing an automatic and objective method for the extraction of cross-sectional slices, which are ensured to be with a correct incline to the surface.

2.1.1 3D model generation

A typical skull dataset consists of multiple horizontal slice images at different heights along the entire skull. *Figure 7* and *Figure 5* show the skull' cross-section when intersected by horizontal planes at different Z axis heights.

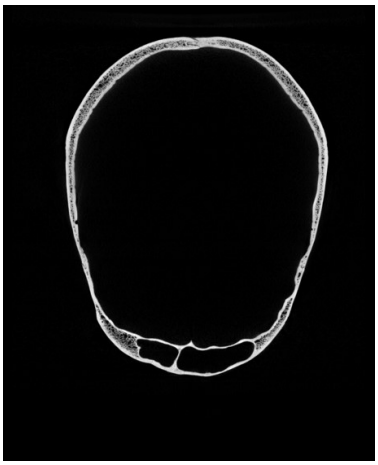

Figure 5: Unprocessed image

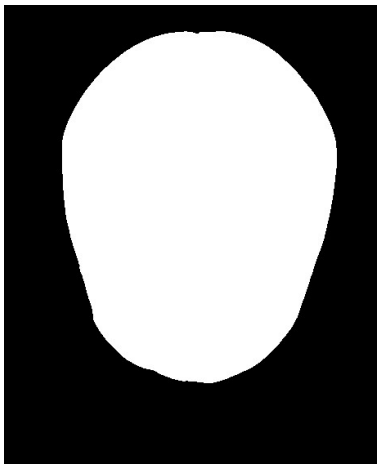

Figure 6: Processed image

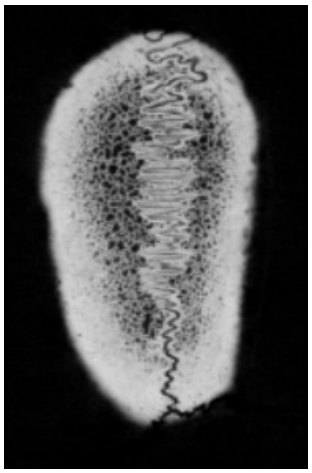

Figure 7

A cross-sectional suture slice at a certain point is defined as an image, perpendicular to the skull' surface at that point. This is not the case with the top of the skull and the provided horizontal slices, as can be seen on *Figure 7*.
To extract cross-sectional suture slices, the algorithm generates a 3D model of the skull, for the user to mark the suture path on. For RAM memory efficiency, a down-scaled version of the volume is loaded, instead of a full sized one.

Take every horizontal slice from the skull volume with dimensions:

$$Width \times Height$$

$z \in (0, 1]$, where z is a variable depending on user preferences

Resultant image with dimensions: $(Width \times z) \times (Height \times z)$

The scale factor has also been taken into consideration with the number of images in the dataset (Z axis), as every $\frac{1}{z}$ th image is loaded. Every down-scaled image is processed through a binarization and hole-filling algorithm as shown in *Figure 5* and *Figure 6*. This removes any unnecessary interior data points in the model, making it easier to generate.
The MATLAB function **isosurface** is used to generate the 3D model from the processed horizontal slices. After the model generation, the user manually selects points of interest defining a particular suture as shown in Figure 2 in the appendix.

2.1.2 Path finding

The next task is to generate the path that the suture follows from the given defining points. Each point on the surface, on the very low level, is part of a triangular mesh, as shown in *Figure 9*.
The question is, which path of connected points on this mesh to take, in order to get from the start to the end point? A novel geometric approach has been used for the task. The chosen method is able to accurately find a path that goes through all given defining points, required to be a minimum of **3**. Let's first look at the simplest case with only three defining suture points.
A line is drawn between the start point A and the end point B. The foot of the normal (the blue line) to the vector $\overrightarrow{AB}$ from the middle point (O) is found and recorded as the point M, as can be seen on *Figure 8*.

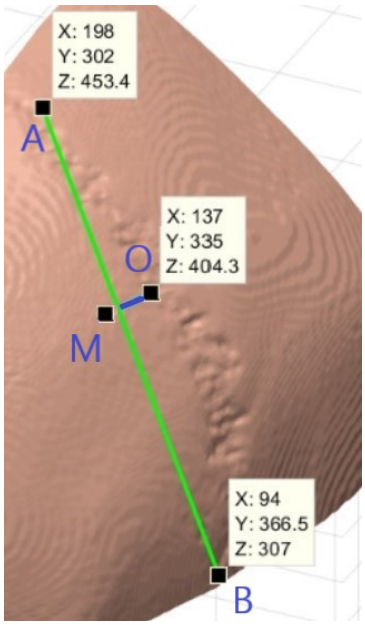

Figure 8: Suture path

$$\overrightarrow{MO} \perp \overrightarrow{AB}$$
$$\overrightarrow{MO} = ?$$
$$|\overrightarrow{AM}| = \frac{\overrightarrow{AO} \cdot \overrightarrow{AB}}{|\overrightarrow{AB}|} \qquad \frac{|\overrightarrow{AM}|}{|\overrightarrow{AB}|} = C$$
$$M = A + C \times \overrightarrow{AB}$$
$$\overrightarrow{MO} = O - M$$

Let's call the vector connecting the foot of the normal M and the middle point O the *compare vector*. This is represented by $\overrightarrow{MO}$.
Starting the path search from the top point A, the normal to $\overrightarrow{AB}$ for each connected vertex is found and recorder as the **current vector**. The next chosen point is the point which has its **current vector** making the smallest angle with the **compare vector**. The process is repeated until the end point is reached. For more complicated cases with

multiple defining points, every three neighboring points are treated as separate cases of the described above. As the algorithm reaches the end point of one such triplet of points it starts to follow the **compare vector** of the next triplet. **j** equidistant points for image generation are extracted from the determined path, where **j** is the number of required cross-sectional images. The described algorithm takes the following mathematical notation:
Let S be the polytope representing the skull's 3D model

$$S \in (x, y, z) : \left\{ \begin{array}{c} x \geq 0 \\ y \geq 0 \\ z \geq 0 \end{array} \right\}$$

The polytope induces a graph with a set of vertices, the vertices of *S(V)*, and a set of edges, the edges of *S(E)* . Furthermore, we can induce a 2 dimensional structure of incidence as the triangle faces of *S(F)*.

$$E \subseteq V^2 \qquad\qquad F \subseteq V^3$$

Introduce the following notation:
$N(D)$ - The set of vertices directly connected to D
Let $(A, B, O) \in V^3$ be manually defined points on the suture.

$M \in AB : OM \perp AB$

$\forall N_i \in N : /N_iB/ < /AB/$
$N_i^{\perp} : N_iN_i^{\perp} \perp AB, N_i^{\perp} \in AB$

We pick a point $A_{\text{next}} : A_{\text{next}} \in N(A)$
$A_{\text{next}} = N_{\text{i}} : (\overrightarrow{N_i^{\perp}N_i}, \overrightarrow{MO})$ is minimal

The blue marks on the skull surface in *Figure 10* represent points of image generation, generated through the described methodology.

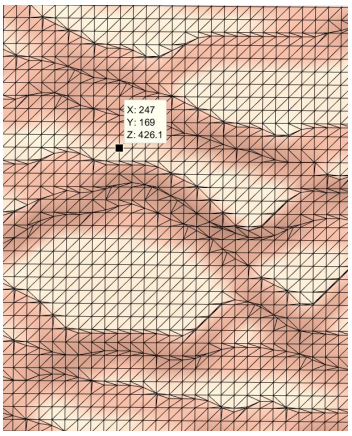

Figure 9: Triangular mesh

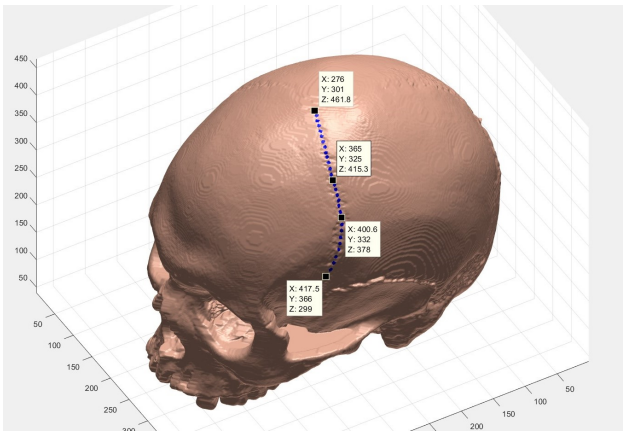

Figure 10: Points of image generation

2.1.3 Surface normal calculation

The next step is to determine at what angle to the skull' surface should an image be generated, in order to correctly represent the cross-section. Let's call the point on the surface, for which a cross-sectional image is required, a **point of interest**. To express the orientation of every image at a **point of interest**, the normal vector of the tangential to the surface plane is used. To find such vector, the **N** closest points to the point of interest are found from the triangular mesh using a **KNN** [6] search algorithm. The value of **N** depends on user preferences, but experimentally it has been determined that a value of $\mathbf{N = 20}$ is sufficient with respect to computational time and accuracy of the produced normal vector. A comparison between surface normals produced with different values of **N** can be found in the appendix on *Figure 3*. The normal vector of each triangle formed by any of the found **N** points is calculated by taking the cross-product of its vertex vectors. The surrounding triangular mesh used for calculating a single surface normal at a **point of interest** is shown in *Figure 4* in the appendix. Every calculated normal vector is scaled with

the area of its origin triangle and ensured to be pointing outwards to the surface. The mean value of all surrounding triangle normal vectors is taken as the best surface normal approximation.

A plane, parallel to the normal vector, is used to extract cross-sectional data from the volume. The algorithm automatically loads the volume in chunks, with a respect to the currently available RAM memory. The generated image planes are intersected with the loaded volume. Color intensity data is extracted from the points of intersection for every plane at a **point of interest**. Every generated image is a plane of volume extracted color intensities.
The loaded volume is made from vertically stacked horizontal images, which are by nature with discrete vertices. A lot of times image planes intersect the volume at non-integer vertex coordinates. To extract color values from the volume at intersection points with non-integer coordinates, bicubic interpolation [3] is used.

2.2 Suture assessment

2.2.1 Suture detection

Once cross-sectional images are generated, to analyze the degree of suture fusion, firstly the suture has to be located on the image. For the purpose, a VGG-16 Semantic Segmentation network [5] for precise suture detection has been used. The network was trained on **6800** manually labeled suture images, which achieves an accuracy of **80.5%** in the suture segmentation. The input size of the network is 256 $\times$ 256 $\times$ 3

Examples of sutures detected by the neural network

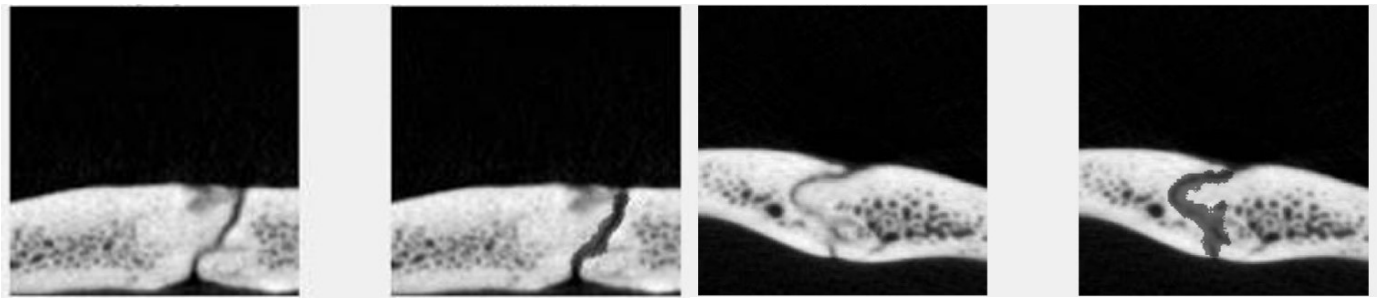

2.2.2 Suture processing

As can be seen, some of the white pixels on the suture boundary are also classified as part of the suture by the neural network. To ensure that the detected area will only contain the actual suture region, the lighter pixels (belonging to the bone) are filtered using triple variable C-Means clustering. The considered variables are - **XY** coordinates of the pixels, and their **color intensity**.

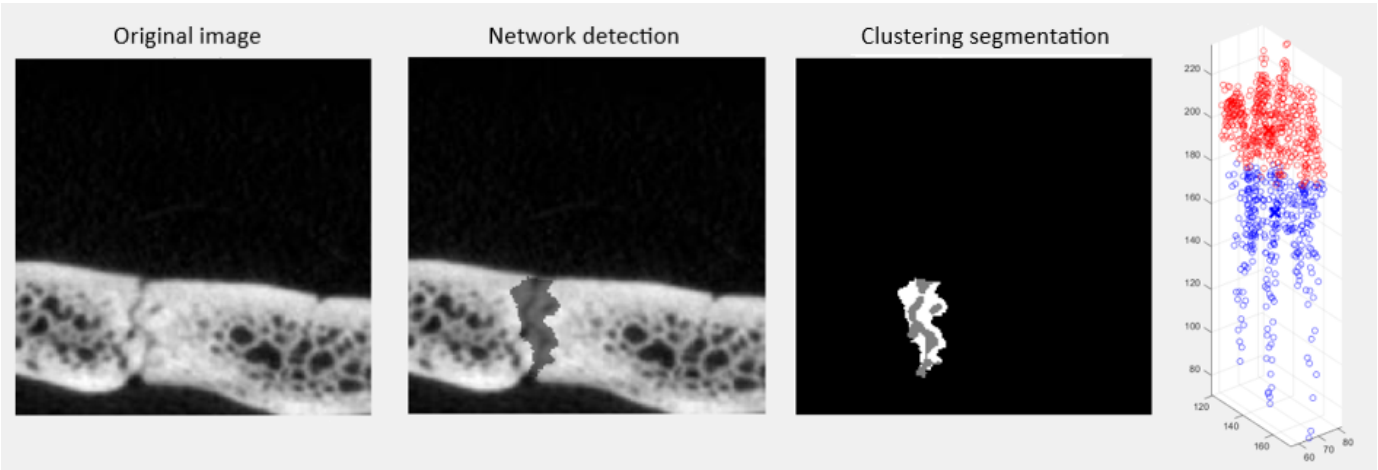

Figure 11: Suture pixels clustering

Number of gray pixels = G
Number of white pixels = W

$$\textbf{Gray ratio} = \frac{\mathrm{G}}{\mathrm{G} + \mathrm{W}}$$

For a low degree of suture fusion, the suture gap is expected to be wide and result in the majority of pixels being classified as **gray**. This would make the ***Gray ratio*** close to 1. Respectively, a fused suture has most of it's area ossified into bone, which has a light color and would be classified as **white** during the clustering segmentation. This would make the ***Gray ratio*** closer to 0, due to the lower fraction of pixels being classified as **gray**.
This segmentation is repeated twice, by clustering the **Gray** classification result from the previous clusterization. This ensures a maximum filtration of white particles and provides several readings for the ***Gray ratio*** metric.

2.2.3 Diploë filtering

Bone diploë particles are present in the entire skull cross-section. Often the segmentation network can mistakenly classify them as being part of the suture, especially if they happen to be positioned near the suture path.
Figure 11 shows a good example of bone diploë being classifies as a suture (The gray colored particle to the right of the suture path is diploë). To account for this error, advantage has been taken of the circular nature that the diploë particles possess. For each individual segmented element, the minimum boundary circle around is calculated. The **particle circularity** is measured.

$$\text{Particle Circularity} = \frac{\text{Particle area}}{\text{Minimum bound circle area}}$$

The more circular a particle is, the more likely it is to be diploë and not part of the suture. After experimentation, it was determined as effective to discard particles with **particle circularity** larger than **0.7**.

2.2.4 Metrics measurement

After the clear segmentation of the suture and the removal of any miss-classified particles, the algorithm measures a number of important metrics used to describe the degree of suture fusion. To examine each skull, 350 cross-sectional suture images along the length of the sagittal suture have been assessed. Throughout the images for every skull, are measured the **standard deviation**, the **median** and the **mean** of each described metric:

- After clustering, the ratio $\frac{\text{Number of } \textbf{gray pixels} \text{ in suture region}}{\text{Total number of pixels in suture region}}$ is measured as the **Gray ratio**. More details about the calculation process are explained in the beginning of *Suture processing*.
- The average color intensity of the suture region marked as the **Color coefficient** metric. It is calculated by taking the mean color value of all pixels classified as a **gray** after clusterization.
  A fused suture consists of mostly solidified bone, which is white and has a high color value. This will increase the value of the metric. The opposite is also true for an unfused suture.
- The average thickness of the suture, measured in pixels is represented by the **suture thickness** metric. This metric is calculated by dividing the number of pixels classified as part of the suture after clusterization by $\frac{\text{Bone area (in pixels)}}{\text{Bone width (in pixels)}}$
  An ossified suture has a much narrower path than an open one, so such metric can introduce useful information.
- The depth of the suture, measured as a fraction from the entire bone cross-section. This metric is marked by **Cross ratio**. In the example, the original image has been processed with the *Canny* [2] edge-detection algorithm. More details about the calculation process of this metric can be found in the appendix under the *Cross ratio measurement* section. The following image is a good representation of how the **Cross ratio** metric is calculated.

$$\text{Cross Ratio} = \frac{\text{X} + \text{Y}}{\text{Z}}$$

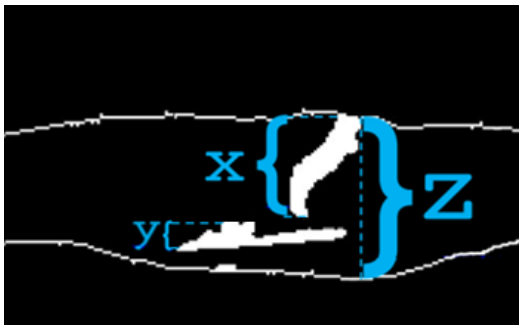

2.3 Measurements outlier filtering

The described above metrics have been collected on each of 350 cross-sectional images for every individual. There are **42 individuals** in the sample. To ensure a minimal error in the assessment, from the 350 values of every metric for a particular individual, any extreme values **z** are filtered out by using the **interquartile method** for outlier filtering.

$$z \in (-\infty, Median - 1.5 \times St.Dev) \cup (Median + 1.5 \times St.Dev, +\infty)$$

2.4 Parameter sensitivity - experimental analysis

The C-Means clustering algorithm requires a parameter called the **partition exponent** in order to perform the segmentation. The following is a comparison of the segmentation achieved by the clustering on the same picture with different values of the **partition exponent** parameter.

Partition exponent = 29

Partition exponent = 14

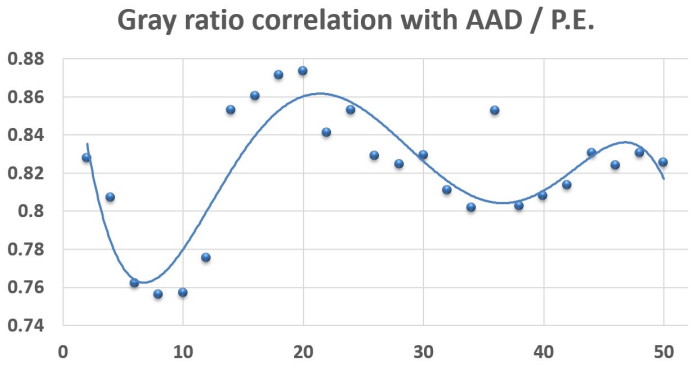

Figure 12

Different values of the clustering *partition exponent (P.E.)* produce different segmentation results. To find the most effective value, the **PMCC** between the **Gray ratio Median** (which depends on P.E.) and Age-At-Death (AAD) has been evaluated for a small group of 13 individuals. This sub-sample was selected on random basis. A total of 25 experiments have been conducted with different and equally spaced values of the *partition exponent*. As can be seen on *Figure 12*, the **PMCC** has the highest value when the partition exponent is equal to approximately **20**. Following the analysis, this is the chosen value for the **P.E.** used to analyze the entire dataset.

3 Project results

The entire skull sample of **42** is split into two groups - the analysis and the test group.

1. The **analysis group** is used for statistical analysis and the creation of a regression equation to estimate the AAD variable with the algorithm's measurements as predictors. This group has a size of 31 individuals from various age groups, chosen on random basis.
2. The **test group** is used to test the regression equation independently and confirm it's accuracy. This groups has a size of 11 individuals from various age groups, chosen on random basis.

The correlation between the Age-At-Death (AAD) of individuals in the sample and the values of the various metrics measured by the algorithm has been evaluated. A hypothesis test based on *PMCC* at the 99.5 % level of certainty, $r = 0.4421$ has been carried out in *Figure 11* in the appendix.
The produced results prove a statistically significant relationship between ***Gray ratio*** and AAD, which has never

been done with the help of an autonomous rating algorithm so far. Interpreting this result implies that by considering a sample of 31 individuals (the *analysis group*), there is 99.5 % chance for the presence of statistically significant correlation between the **Gray ratio** and AAD in the parent population.

3.1 Suture fusion patterns

The following graphs represent the variation in the **suture thickness** metric throughout the consecutive sagittal suture images, measured for three different individuals from the sample. The Y axis corresponds to the **suture thickness** value, and the X axis is the image index along the suture length:

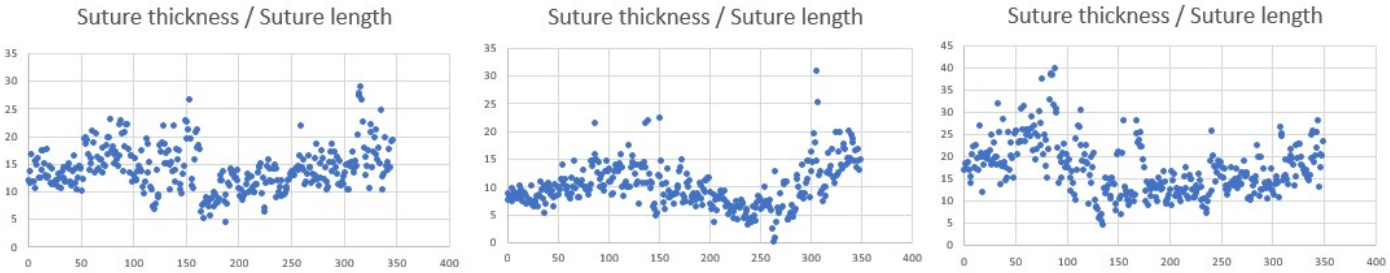

The **suture thickness** measurement along the length of the suture produces a very consistent pattern. On all of the graphs, the **suture thickness** tends to increase towards the end of the suture length. This common graph pattern confirms the validity of the chosen segmentation technique, as this is exactly the type of pattern one would expect the see on a manual suture inspection; the bone ossification is the lowest (corresponding at a high **suture thickness**) towards the end of the suture length, as this is the place where the sagittal suture connects with the lambdoid suture. This graph comparison is an important analysis of the data, as it shows that the segmentation technique is working in the right direction by confirming the known nature of bone ossification throughout the suture length.

3.2 Regression for AAD estimation

It is a non-trivial task to generate a universal model for precise AAD estimation based only on a sample of total size **42**. Even if created, such model will likely not be very reliable for individuals originating from other samples and populations.
However, the opportunity to find a reliable model for the particular sample is quite an achievable task. Such result has the potential to prove the application of computer algorithms in suture assessment as a valuable alternative to the subjective techniques used so far. To confirm such potential uses, a statistically significant correlation has been shown between multiple autonomously measured variables and AAD, which is displayed on the following graphic.

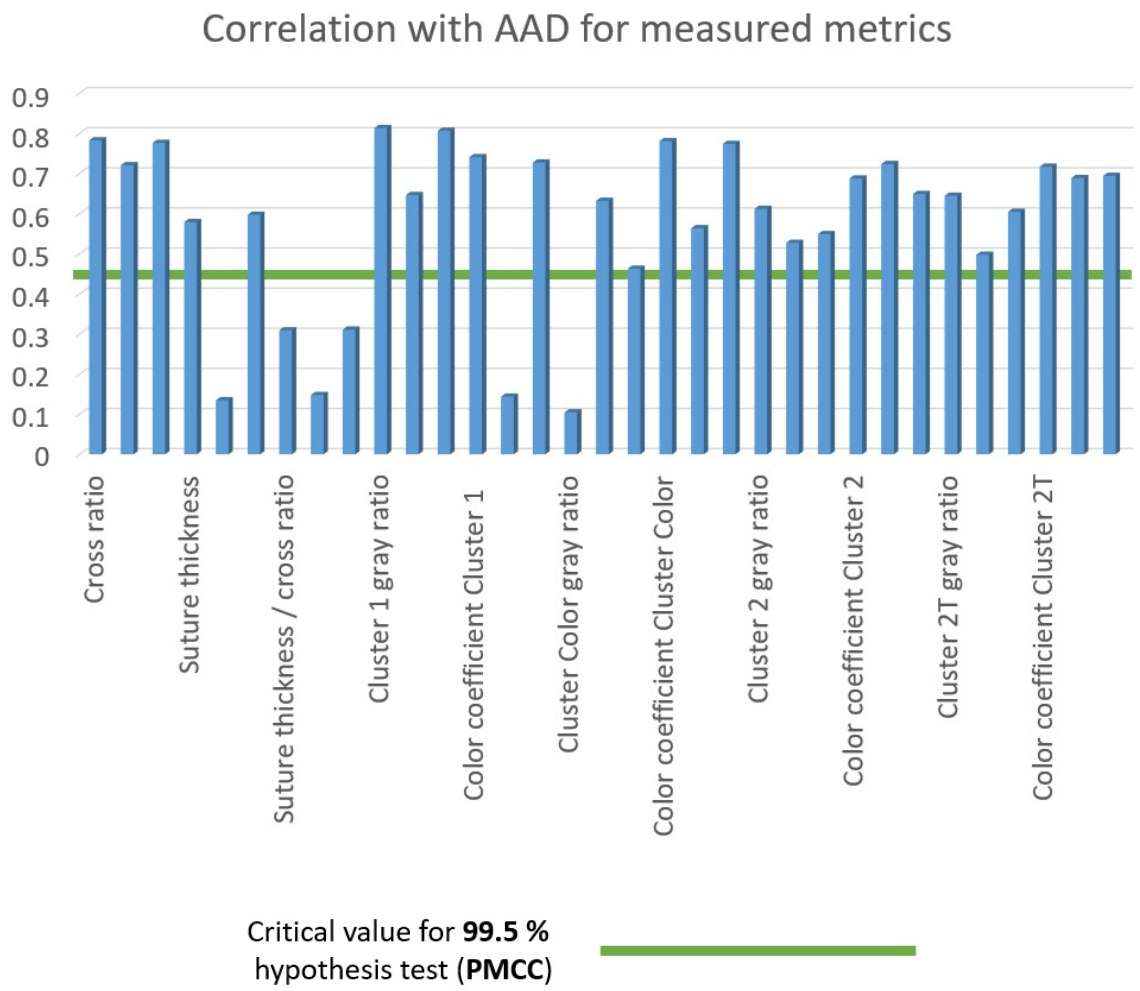

The non-redundant variables with a statistically significant **PMCC** (above the critical value) have been used to form a regression model for AAD estimation. The model's equation has been generated with *Minitab* through forward step regression of the *analysis group*.

$$\textbf{Predicted age} = 937X_2 - 1098X_2^2 - 45.5X_3 - 29.52X_1 - 118.9$$

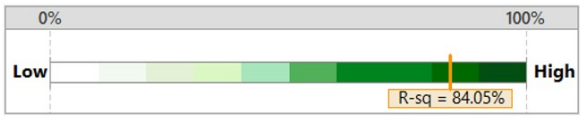

R^2 = 84.05 %

84.05 % of the variation in the response variable Age-At-Death can be explained by the model

X1: Cross ratio Mean *X2: Gray ratio 1 Median* *X3: Color coefficient C Mean*

The regression has been ran through the *test group*, which is entirely independent of the *analysis group* used to generate the model. This ensures the results are not due to over fitting the particular dataset.

As the size of the sample is larger than 30 individuals, by the **central limit theorem**, the AADs in the sample can be approximated using a Normal distribution. A **95% confidence interval** is produced for each entry. In this case, the confidence interval represents the mean AAD for a population of individuals having the same particular metric values. For example, if a sample of 20 individuals with the same metric values is taken, it is expect that the mean AAD for individuals with such metric values lies in 19 of the confidence intervals with the same level of certainty for the AAD of every sampled individual. This relationship is visualized on *Figure 12* in the appendix.
Applying the generated model on the *test group* produces the following *AAD* estimates:

Actual AAD	Predicted AAD	95% Confidence Interval	X_1	X_2	X_3
55	52	(46.5763, 57.3809)	0.25773	0.37903	0.41568
47	49	(46.2747, 52.6537)	0.55772	0.40657	0.32112
45	47	(44.4301, 50.0228)	0.53233	0.38353	0.35173
41	40	(35.3710, 44.6550)	0.73413	0.47496	0.36764
30	33	(30.2521, 35.2103)	0.81460	0.46502	0.49639
33	34	(30.9351, 36.3297)	0.89114	0.44582	0.45360
29	32	(29.4806, 34.8996)	0.88999	0.45257	0.47871
21	20	(16.6788, 24.1885)	0.94014	0.49777	0.59869
24	21	(16.8168, 25.4547)	0.86749	0.50847	0.59086
19	18	(14.2285, 22.7227)	0.97389	0.50968	0.57547
48	40	(33.9990, 46.7352)	0.50132	0.44309	0.56098

3.3 Outliers

Just like with anything, there always are outliers to the model predictions, as can be seen on the last example in the table. To investigate how strong the presence of outliers is according to the model, a residual plot has been created from which the *Standard Error* of the model during fitting has also been deduced. The plot is displayed on *Figure 13* in the appendix. There are only 2 unusual values (blue and red square) out of the 31 used to fit the model. From the *test group* there is only 1, if the **Interquartile range** method of outlier identification is used. A total of **3 residuals** to the model out of the total 42 samples, suggests that more than 90% of the individuals in the sample possess sutures reliable for the age estimation. This number certainly suggests that the chosen methodology is reliable for this particular set. Furthermore, the **Standard Error** of the regression is relatively low for the sample when compared to the **S.E.** produced by existing studies. The potential causes for outliers underlie in the known nature of suture ossification.

- Similarly to puberty, the process of suture ossification can occur earlier in some individuals than in others, opening the possibility for a unique ossification pattern in different individuals. This can't always be taken into account by a generalized prediction model.
- If an individual is systematically exposed to starvation, it is likely that their bones are underdeveloped for their age. Also, conditions like osteoporosis can significantly affect the degree of suture fusion.

Many external factors as such, can't always be taken into account, especially when working with an old sample. This can cause some inaccuracy, which is of course inevitable regardless of the age estimation method.

3.4 Results summary

Considering that the most accurate already existing methods for AAD estimation based on analysis of the cranial sutures have an error of + / - 15 year, the achieved results show a significant improvement. Judging by the amount of available data, the project manages to reduce the error of the predicted AADs over 3 times compared to the already existing techniques.
It is hard to conclude with certainty whether or not the achieved result and methodology can be used reliably in practice, as the sample size is limiting. However, the statistical analysis and hypothesis testing certainly show a significant relationship between the measured variables and AAD, which is an important result for the future development of cranial suture analysis algorithms. In conclusion, the algorithm completely automatizes the process of cranial suture assessment and suggests to be more accurate than the already existing methods for age estimation based on cranial suture analysis. The presented methodology can be used for analyzing skulls of any ethnicity after appropriate tuning of the regression equation, making the algorithm applicable in a wide variety of fields including criminology and archaeology.